SAND2010-1131C

Readout IC requirement trends based on a simplified parametric seeker model

Thor D. Osborn*

Sandia National Laboratories, P.O. Box 5800, MS 0892, Albuquerque, NM, USA 87185-0892

ABSTRACT

Modern space based optical sensors place substantial demands on the focal plane array readout integrated circuit. Active pixel readout designs offer direct access to individual pixel data but require analog to digital conversion at or near each pixel. Thus, circuit designers must create precise, fundamentally analog circuitry within tightly constrained areas on the integrated circuit. Rapidly changing phenomena necessitate tradeoffs between sampling and conversion speed, data precision, and heat generation adjacent the detector array, especially of concern for thermally sensitive space grade infrared detectors. A simplified parametric model is presented that illustrates seeker system performance and analog to digital conversion requirements trends in the visible through mid-wave infrared, for varying sample rate. Notional limiting-case Earth optical backgrounds were generated using MODTRAN4 with a range of cloud extremes and approximate practical albedo limits for typical surface features from a composite of the Mosart and Aster spectral albedo databases. The dynamic range requirements imposed by these background spectra are discussed in the context of optical band selection and readout design impacts.

Keywords: FPA, ROIC, ADC, MWIR

1. INTRODUCTION

Many layers of complexity must be embraced in the proper design and development of space based optical sensors. But the intuitive comprehension of system performance drivers needed by many stakeholders in the development process may be obfuscated. The following analysis links seeker performance constraints to analog-to-digital converter (ADC) effective bit count requirements for a nadir-pointing satellite-mounted optical sensor operating within the Vis-MWIR band. This highly simplified model favors heuristic benefit over strict quantitative accuracy in the hope of broadening information exchange among the various contributors, including the sensor engineering, program oversight and component development communities.

2. SEEKER MODEL

2.1 Simplified seeker construct

A highly simplified optical seeker or warning sensor is depicted schematically in Figure 1 below. This sensor seeks for

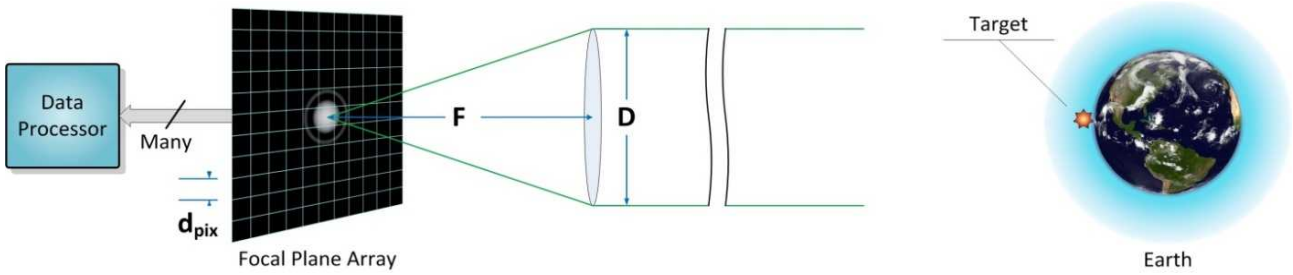

Figure 1. Simplistic optical seeker sensor.

* tdosbor@sandia.gov; phone (505) 845-8786

targets of interest on or near the surface of the Earth. These targets may be ground-based, atmospheric, or exo-atmospheric. The distance between the sensor aperture D and the target is assumed large enough that the target may be treated as a point source (*i.e.,* will not be resolved) and the difference between aperture-target and aperture-Earth distance is negligible. The FPA is assumed to be cooled sufficiently to support background limited performance. The Earth's black body and reflected solar emissions set an unavoidable floor on the background photon flux, hence photon noise, as long as the target remains between the sensor field of view (FOV) and the Earth. Target detection depends fundamentally on the ratio of target emissions to the noise contributed by Earth background emissions captured on a detector pixel within the focal plane array (FPA).

Both target emission capture efficiency and the Earth background spectrum may be estimated with reasonable accuracy. The FPA pixel sample noise is fundamentally limited by the background emissions. Consequently, analysis of target emission capture could be minimized in the determination of ROIC requirements. Parameterization of the target capture aspect of sensor design, however, provides a unifying link between sensor design objectives, telescope parameters, and the optical background captured by a detector pixel, enabling a cohesive assessment of requirement trends.

2.2 Normalized Airy point spread function

The Airy point spread function (PSF) characterizes the diffraction pattern produced at the focal plane when point source emissions such as the aforementioned target are collected by a circular aperture and focused to a spot. The power distribution function is:

$$E(m,\lambda) = \phi_\lambda \cdot \pi \cdot \left(\frac{NA}{\lambda}\right)^2 \cdot \left[\frac{2 \cdot J_1(m)}{m}\right]^2 \tag{1}$$

where ϕ_λ is the total incident power within the distribution at wavelength λ, and

$$m = 2 \cdot \pi \cdot \left(\frac{NA}{\lambda}\right) \cdot r \tag{2}$$

Assuming the optical train is not ultra-fast, the numerical aperture may be approximated as:

$$NA \approx \frac{1}{2 \cdot f_\#} \tag{3}$$

where $f_\# = F/D$, and F is the effective focal length of the telescope. The first zero of the Bessel function in Equation (1) occurs when $m = 3.83$ and defines the radius of the Airy disc as $r_{Airy} = 1.22 \cdot \lambda \cdot f_\#$, thus:

$$D_{Airy} = 2.44 \cdot \lambda \cdot f_\# \tag{4}$$

For systems calibrated to match the Airy disc produced by a target point source to the focal plane array pixel dimensions we have:

$$D_{Airy} = n \cdot d_{pix} \tag{5}$$

Where n is the pixel span of the Airy disc. It follows that:

$$d_{pix} = \frac{2.44 \cdot \lambda \cdot f_\#}{n} \tag{6}$$

A normalized Airy radius may then be defined that enables reformulation of the Airy power distribution and simplification of the expression for the power captured by a detector pixel (next section):

$$r_{norm} = \frac{m \cdot n}{\pi \cdot 2.44} \tag{7}$$

Incorporating the pixel-normalized radius, a normalized and more illustrative form of Equation (1) is obtained:

$$E(r_{norm}, n) = \frac{\phi_\lambda}{\pi \cdot r_{norm}^2} \cdot J_1^2\left(\frac{\pi \cdot (2.44) \cdot r_{norm}}{n}\right) \tag{8}$$

Visualization of this normalized Airy point spread function is presented in Figure 2 below.

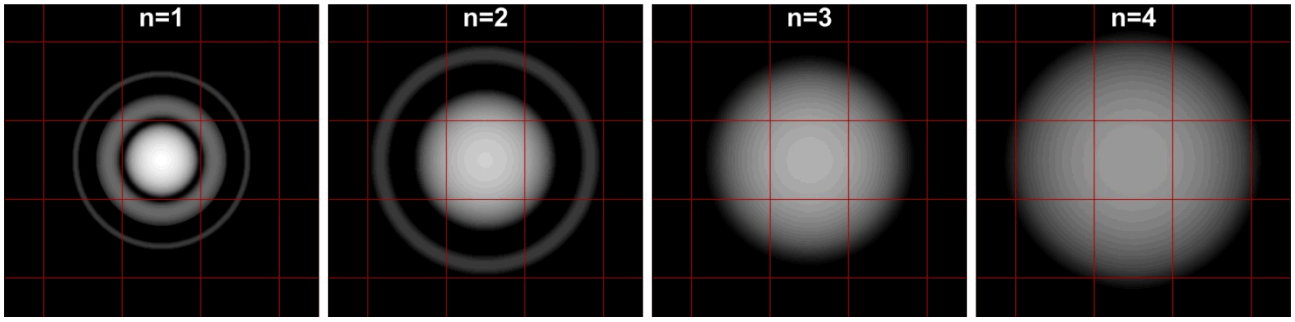

Figure 2. Airy point spread function normalized to focal plane array pixel size. Grid represents pixel edges.

2.3 Normalized pixel ensquared energy

The *ensquared* energy fraction of the Airy PSF that is captured by a square detector pixel in the focal plane array determines the signal amplitude produced by a point source target. The Airy PSF is radially symmetric and the central disc may be approximated by an error function profile. Consequently, for an Airy PSF with its centroid at the center of a detector pixel and a pixel span of $n = 1$, the corner regions of the ensquared PSF represent little energy content relative to the *encircled* PSF of the corresponding inscribed region. In this circumstance we can estimate the diffraction-limited ensquared energy using the corresponding encircled energy, for which a Bessel function solution is available:

$$EE \cong 1 - J_0^2\left(\frac{\pi \cdot D \cdot IFOV}{2 \cdot \lambda}\right) - J_1^2\left(\frac{\pi \cdot D \cdot IFOV}{2 \cdot \lambda}\right) \tag{9}$$

where IFOV is the instantaneous[†] field of view of a pixel, approximated as d_{pix} / F. Alternatively, Equation (9) may be written in terms of the optical train $f_\#$ and d_{pix}, the FPA pixel detector width:

$$EE \cong 1 - J_0^2\left(\frac{\pi \cdot d_{pix}}{2 \cdot \lambda \cdot f_\#}\right) - J_1^2\left(\frac{\pi \cdot d_{pix}}{2 \cdot \lambda \cdot f_\#}\right) \tag{10}$$

Equation (6) may be re-written:

$$\frac{d_{pix}}{f_\#} = \frac{2.44 \cdot \lambda}{n} \tag{11}$$

Thus enabling generation of a simplified and normalized encircled energy function:

$$EE(n) = 1 - J_0^2\left(\frac{\pi \cdot 1.22}{n}\right) - J_1^2\left(\frac{\pi \cdot 1.22}{n}\right) \tag{12}$$

The ensquared energy may also be calculated via numerical integration, and the normalized encircled and ensquared energies are plotted in Figure 3. The differences are very modest when the pixel size is approximately equal to the size of the disc, because the additional areas captured by the corners of the square pixel contain very little flux, but as the

[†]The term *instantaneous* refers to the pixel field of view in a scanning linear detector array. *Incremental* would be more logically appropriate for staring FPAs, but would not change the accepted acronym.

relative size of the disc increases the region of high flux density is pushed outward to the corners of the square pixel while simultaneously an increasing fraction of the flux falls outside of the edges of the pixel. Therefore, in the specific case of an Airy PSF centered on a pixel of interest, the encircled energy is an excellent estimate for small n and a passable estimate for larger Airy disc pixel spans.

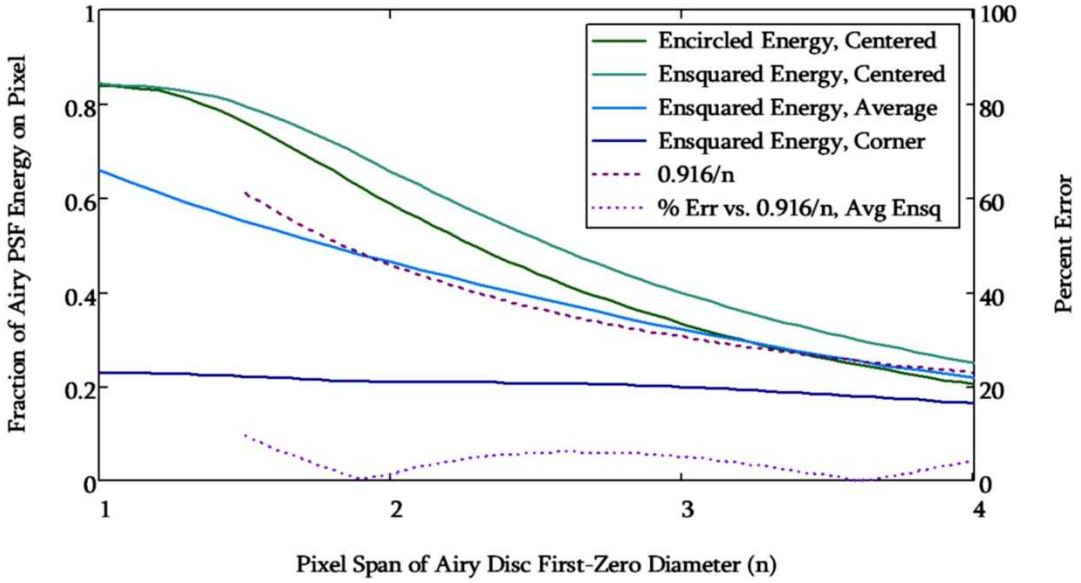

Figure 3. Pixel energy capture versus normalized Airy disc diameter.

In general, however, the position of the Airy disc produced by target emissions will not be aligned to the centroid of a detector pixel. There is equal probability of the disc being centered on any location within the most central pixel. The average ensquared energy as estimated by the Monte Carlo method is also plotted in Figure 3. For pixel spans of $1.5 \le n \le 4$ the average ensquared energy may be approximated to within 10% by $0.916 / n$.

The relationship between the pixel-normalized Airy PSF and image quality for imaging sensors has been discussed by Lomheim and Hernàndez-Baquero[1]. Here, in the context of a seeker system, the target is treated as a point source and the captured photon intensity is the important relationship for detection purposes. Although energy capture, hence SNR, is maximized for small n, other practical constraints lead sensor designers to more typically use values in the range of $1.5 \le n \le 3$. For example, spreading the Airy disc across multiple pixels offers mitigation against single defective pixels, a common FPA imperfection. A broader distribution may also be chosen to enable sub-pixel estimation of target location[2]. Consequently, the choice of n is a key design decision involving multiple engineering trade-offs. Once chosen, by Equation (11) the design space for the detector array and telescope are constrained, thereby also placing constraints on background flux collection.

3. BACKGROUND ESTIMATION

Regardless of the quality of the optical intake train, detector, and readout electronics, the background emissions of the Earth constitute an irreducible and ultimately performance-limiting source of noise. For a nadir-pointing sensor the Earth appears as a dynamic patchwork of various background types with characteristic emission spectra that depend on surface and atmospheric properties, latitude, time of day, temperatures, *etc.* One of the key factors influencing the effective background radiance of a region of the Earth's surface is the dramatic variation in characteristic reflectance spectra of the landscape depending on soil and vegetation types as well as artificial structures. Spectral albedo data have been collected for a wide variety of terrains and surface features[3-4]. The spectral albedo chart in Figure 4 gives extreme values generated from spectra of a variety of land and water surface features[‡]. Although wider extreme values may exist and could certainly be contrived, these limits should be more representative than simply choosing unity and zero.

[‡] Specifically, for land, from the Mosart database: Pine Forest, Evergreen Broadleaf Forest, Deciduous Needle Forest, Deciduous Broadleaf Forest, Mixed Forest, Antarctic Snow, Barren Desert, Closed Shrubs, Cropland, Crop Mosaic, Fresh Snow, Grassland,

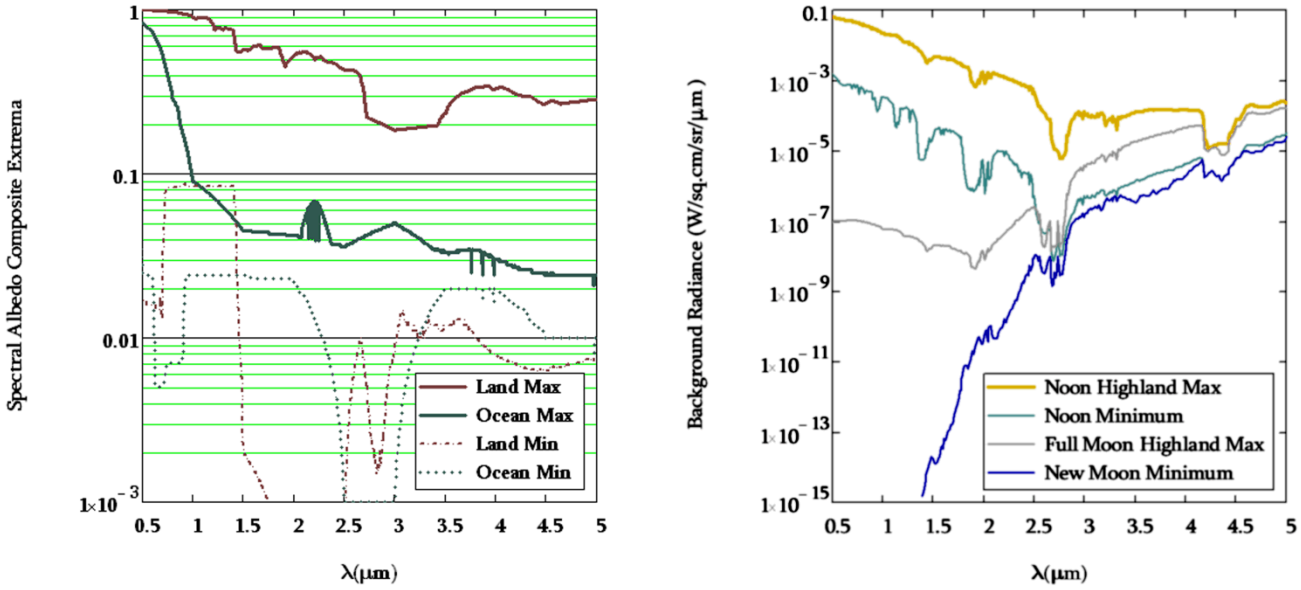

Figure 4. Spectral albedo and modeled Earth background radiance extrema.

The spectral albedo chart above (left) gives approximate limits on the assumed Lambertian reflectance of the Earth's surface features. The emissions reaching space depend on a host of variables including atmospheric conditions, geometric factors, cloud cover and type, latitude, season, *etc.* In order to estimate background emissions from the vantage of a nadir-pointing optical sensor in space, simulation software was utilized. The above albedo spectra were provided to MODTRAN4 (version 3, revision 1, obtained from Ontar Corporation, North Andover, MA) and a virtual design of experiments comprised of more than 1600 separate simulation runs was performed to estimate maximal and minimal Earth background spectra across latitude, season, surface feature altitude, observation angle, and time of day. Sample results representing extreme background radiance values are also given in Figure 4 (right).

4. CAPTURED BACKGROUND FLUX AT THE DETECTOR

The background emissions of the Earth were presented in terms of power in Figure 4 above. Given that charge carrier generation in typical semiconductor-based detectors is a function of photon absorption, and that background noise calculation is more straightforward using captured charge counts, the photon flux is more useful in the following analyses than the power flux. The photon background radiance of the Earth within an optical band of interest is:

$$L_{q,Earth} = \int_{\lambda_{lo}}^{\lambda_{hi}} L_{Earth}(\lambda) \cdot \frac{\lambda}{hc} \cdot d\lambda \tag{13}$$

The photon background flux per pixel that reaches the FPA is found by combining Equation (13) with considerations of optical throughput and the transmissivity of the optical train in the band of interest. The throughput is represented by the product of the areas of the pixel and optical aperture divided by the square of the focal length. The transmissivity of the optics is a function of λ, although for sufficiently narrow optical bands it may be approximated as a constant. For a nadir ground sample distance (GSD) on the Earth matched through telescope optics to a detector pixel, the flux capture is:

Savanna, Tundra, Urban, Wetland, Woody Savanna. Additional spectra from the Aster database include: Asphalt, Coarse Granular Snow, Dry Grass, Fine Snow, Frost, Granite, Medium Granular Snow, Pale Brown Silty Loam, Paving Concrete, Sandy Loam, Very Dark Grayish Brown Loamy Sand, Very Dark Graying Brown Silty Loam, Very Pale Brown to Brownish Yellow Interior Dry Gravelly Silt Loam, and White Gypsum Dune Sand. For water, Mosart database values for sea ice and ocean water as well as Aster database values for sea foam and sea water.

$$\Phi_{qbg,pix} = \int_{\lambda_{lo}}^{\lambda_{hi}} \left(\frac{GSD^2 \cdot \pi \cdot \frac{D^2}{4}}{\rho_{alt}^2} \right) \cdot \zeta_{optics}(\lambda) \cdot L_{q,Earth}(\lambda) \cdot d\lambda \tag{14}$$

However, to an extremely good approximation, $IFOV = d_{pix} / F$ and $GSD = IFOV \cdot \rho_{alt}$, therefore:

$$\Phi_{qbg,pix} = \int_{\lambda_{lo}}^{\lambda_{hi}} \left(\frac{d_{pix}^2 \cdot \pi \cdot \frac{D^2}{4}}{F^2} \right) \cdot \zeta_{optics}(\lambda) \cdot L_{q,Earth}(\lambda) \cdot d\lambda \tag{15}$$

The normal intuitive expectation of a ρ_{alt}^2 dependence on flux capture has not been lost. Rather, in the formulation of Equation (15) it is implicit that the solid angle captured by a single pixel is fixed. Therefore, GSD increases in tandem with altitude, so that the net flux capture on a per-pixel basis does not change for backgrounds with low spatial variation, although rapidly-changing terrain background radiances will be blurred together due to the increased GSD.

The band-limited background photon flux obtained in Equation (15) enables calculation of the charge collection of a single pixel during one sample period. The optical band of interest is assumed to be sufficiently narrow that the quantum efficiency, $\eta(\lambda)$, of the detector will be approximately constant over that band and may be represented by its average value, $\overline{\eta}$. The background charge generation rate of the detector will be the product of the quantum efficiency, the background photon flux, and the unit charge. Multiplication of this rate by the nominal sample integration time τ_{int} would ideally give the per-sample background charge accumulation, but a portion of the sample time is lost to resetting the sample integration well and other pixel-level electronic circuitry. Therefore a duty factor, δ, must be included:

$$Q_{bg,pix} = \tau_{int} \cdot \delta \cdot \overline{\eta} \cdot q \cdot \Phi_{qbg,pix} \tag{16}$$

The pixel background photon noise is then:

$$\sigma_{bg,pix} = \sqrt{q \cdot Q_{bg,pix}} \tag{17}$$

4.1 Normalization of background radiance

Assuming the transmissivity of the sensor telescope is approximately constant over the optical band of interest, Equation (15) may be re-written as:

$$\Phi_{qbg,pix} = \overline{\zeta}_{optics} \cdot \frac{d_{pix}^2}{f_{\#}^2} \cdot \int_{\lambda_{lo}}^{\lambda_{hi}} \left(\frac{\pi}{4} \right) \cdot L_{q,Earth}(\lambda) \cdot d\lambda \tag{18}$$

A set of normalized background incidance spectra, $E_{qnorm,Earth}(\lambda)$, may then be generated, for which the rate of photon arrival at a detector pixel is found simply by multiplying the normalized integrated spectral value by the correction factors external to the integral:

$$\Phi_{qbg,pix} = \overline{\zeta}_{optics} \cdot \frac{d_{pix}^2}{f_{\#}^2} \cdot \int_{\lambda_{lo}}^{\lambda_{hi}} E_{qnorm,Earth}(\lambda) \cdot d\lambda \tag{19}$$

Applying Equation (16), the pixel background charge collected per sample may be found, effectively bounding the noise floor of the sensor for detection of rapid events:

$$Q_{bg,pix} = \tau_{int} \cdot \delta \cdot \overline{\eta} \cdot q \cdot \overline{\zeta}_{optics} \cdot \frac{d_{pix}^2}{f_{\#}^2} \cdot \int_{\lambda_{lo}}^{\lambda_{hi}} E_{qnorm,Earth}(\lambda) \cdot d\lambda \tag{20}$$

As with any simplified model, certain limitations apply. If a single pixel represents a large ground sample distance on the earth, then over most geographic areas a weighted average of many terrain types will be captured. Similarly, if the $f_{\#}$ is large, then the background terrain mapped by the pixel will necessarily be heavily blended with or even dominated by the emissions of adjacent background areas through blurring. Nevertheless, the idealized spectra still represent informative bounding cases for assessing noise floor and readout circuit integration well depth design requirements.

Consider a sensor designed for maximum background conditions. The normalized maximum daytime background, integrated over various optical bandwidths, is provided in Figure 5 (left) below. The integration bandwidths are centered around nominal λ. Optical background may be minimized by filtering for specific narrow bandwidths, and SNR will be enhanced if the effective target emissions coincide with one of the background minima. Conversely, a sensor may be designed to dynamically attain the greatest practical sensitivity for the extant background conditions at a given moment. For example, there may be an interest in detecting events at night that would be obscured during the daytime. The chart at right in Figure 5 provides the normalized band-limited maximum nighttime background. Substantial background differences must be accommodated at wavelengths below about 4 μm.

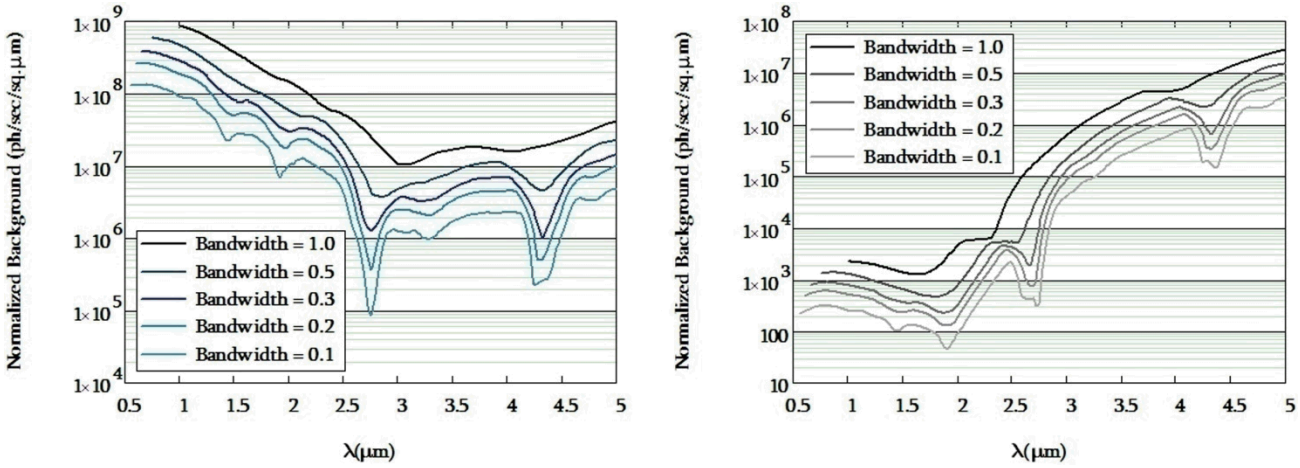

Figure 5. Normalized integrated maximum Earth background incidances. Highland noon (left) and full moon midnight (right).

5. EFFECTIVE BIT COUNT REQUIREMENTS FOR ROIC ADC

5.1 Required performance based on well size and dynamic range

ADC noise theory, quality metrics, and empirically demonstrated performance trends have been thoroughly explored elsewhere[5-6]. The analog voltage that maps to a single digital bit (least significant bit, or LSB) is:

$$\Delta V_{LSB} = \frac{V_{FS}}{2^{N_{bits}}} \tag{21}$$

where V_{FS} is the full-scale voltage. Quantization is the only noise produced by an ideal ADC, and it is not, strictly speaking, random. On a practical basis, however, it will appear to be random if the signal is complicated or carries even modest random noise. This quasi-random quantization noise is estimated as:

$$\sigma_{v,ideal} = \frac{V_{FS}}{2^{N_{bits}} \cdot \sqrt{12}} \tag{22}$$

The equivalent noise charge is better for combination or comparison with photon shot noise. The full scale charge is:

$$Q_{FS} = V_{FS} \cdot C_{int} \tag{23}$$

The term Q_{FS} is also referred to as the integration well size, capacity, or depth. The ADC quantization noise in charge terms is:

$$\sigma_{q,ideal} = \frac{V_{FS} \cdot C_{int}}{2^{N_{bits}} \cdot \sqrt{12}} \tag{24}$$

From a system design perspective, the achievement of BLIP or near-BLIP performance demands that the ADCs have sufficient effective bit count such that the ADC noise contribution does not exceed that of the inherent background. Substitution of an allowed noise and effective bit count into Equation (24) yields, with appropriate rearrangements:

$$N_{eff} = \log_2 \left[\frac{V_{FS} \cdot C_{int}}{\sigma_{q,allowed} \cdot \sqrt{12}} \right] \tag{25}$$

By definition, $\sigma_{q,allowed}$ is determined by the photon background under BLIP conditions (*i.e.*, $Q_{bg,pix}$). At initial detection the target signal is expected to be negligible in comparison. The minimum integration well charge depth is the sum of the maximum background and target emissions: $Q_{FS,min} = Q_{bg,pix} + Q_{targ,max}$. Given that targets of interest are highly specific to the sensor application, with widely varying spectral structures and intensities, this unknown will be treated parametrically as $\varepsilon = Q_{targ,max} / Q_{bg,pix}$. In photon terms, canceling common efficiency factors, this quotient is:

$$\varepsilon = \int_{\lambda_{lo}}^{\lambda_{hi}} \zeta_{atm}(\lambda) \cdot I_{q,targ}(\lambda) \cdot d\lambda \Big/ \int_{\lambda_{lo}}^{\lambda_{hi}} L_{q,bg}(\lambda) \cdot d\lambda \tag{26}$$

The minimum well size is then:

$$Q_{FS,min} = Q_{bg,pix} \cdot (1 + \varepsilon) \tag{27}$$

Since poisson statistics apply, $q \cdot Q_{allowed} = \sigma^2_{q,allowed}$, thus:

$$\sigma_{q,allowed} = \sqrt{\frac{q \cdot Q_{FS,min}}{1 + \varepsilon}} \tag{28}$$

Substituting into Equation (25) we obtain:

$$N_{eff} = \tfrac{1}{2} \cdot \log_2 \left[\frac{Q_{FS,min} \cdot (1 + \varepsilon)}{q \cdot 12} \right] \tag{29}$$

The relationship in Equation (29) will yield a reasonable estimate for the necessary effective bit count of the ADC in the case of a fixed integration well and consistent mean photon background. If the background level is inconsistent, however, then in order to maintain instantaneous BLIP the ADC will be required to have additional effective bits to handle the dynamic range introduced by scene variations with lower background levels. Introducing a dynamic range factor $\beta = \Phi_{bg,max} / \Phi_{bg,min}$, $Q_{low} = Q_{allowed} / \beta$, and therefore:

$$\sigma_{q,low} = \sqrt{\frac{q \cdot Q_{FS,min} \cdot (1 + \varepsilon)}{q \cdot \beta \cdot 12}} \tag{30}$$

$$N_{eff} = \tfrac{1}{2} \cdot \log_2 \left[\frac{Q_{FS,min} \cdot \beta \cdot (1 + \varepsilon)}{q \cdot 12} \right] \tag{31}$$

The effect of allowing for a substantial dynamic range in background flux is to demand an additional one-half bit of ADC performance per octave of background fluctuation. The dynamic range for a sensor operating in both daytime and full moon nighttime conditions may be as high as 500,000 depending on the optical band. For space-based sensor systems with both daytime and nighttime applications, the complexity introduced by a selectable dual or multiple well capacitance may be preferable to the taxing design challenges of high bit-count, compact, low-power ADCs if continuous BLIP performance is desired.

5.2 Normalized ADC effective bit count requirements

Given Equation (31) it is possible to estimate the effective number of ADC bits required to support BLIP sensor performance based on the value of $Q_{FS,min}$, the minimum full-scale integration well depth. Combining Equations (20) and (27):

$$Q_{FS,min} = (1+\varepsilon)\cdot\tau_{int}\cdot\delta\cdot\overline{\eta}\cdot q\cdot\overline{\zeta}_{optics}\cdot\frac{d_{pix}^2}{f_{\#}^2}\cdot\int_{\lambda_{lo}}^{\lambda_{hi}} E_{qnorm,Earth}(\lambda)\cdot d\lambda \tag{32}$$

Incorporating Equation (11) and replacing integration time with sample frequency, f_s, the above may be re-written as:

$$Q_{FS,min} = \left(\frac{(1+\varepsilon)\cdot\delta\cdot\overline{\eta}\cdot q\cdot\overline{\zeta}_{optics}}{n^2\cdot f_s}\right)\cdot(2.44)^2\cdot\int_{\lambda_{lo}}^{\lambda_{hi}}\lambda^2\cdot E_{qnorm,Earth}(\lambda)\cdot d\lambda \tag{33}$$

Division by V_{FS} then yields the minimum required integration well capacitance. Insertion of Equation (33) into Equation (31) enables estimation of the ADC bit count requirement, expressed in terms of a correction factor to a normalized requirement (*i.e.*, $N_{eff} = N_{corr} + N_{norm}$) that is independent with respect to sensor design specifics:

$$N_{eff} = \tfrac{1}{2}\cdot\log_2\left[\frac{\beta\cdot(1+\varepsilon)^2\cdot\delta\cdot\overline{\eta}\cdot\overline{\zeta}_{optics}}{n^2\cdot f_s}\right] + \tfrac{1}{2}\cdot\log_2\left[\frac{(2.44)^2}{12}\cdot\int_{\lambda_{lo}}^{\lambda_{hi}}\lambda^2\cdot E_{qnorm,Earth}(\lambda)\cdot d\lambda\right] \tag{34}$$

Doubling n decreases the requirement by one bit. Similarly, doubling the dynamic range or sample frequency increases or reduces the requirement by one-half bit, respectively. The efficiency factors, δ, $\overline{\eta}$, and $\overline{\zeta}_{optics}$ ideally should each approach unity but allowances can be made where this does not hold. The normalized requirements for maximum daytime and maximum full moon Earth background integrated over representative optical bandwidths are provided in Figure 6 at left and right, respectively.

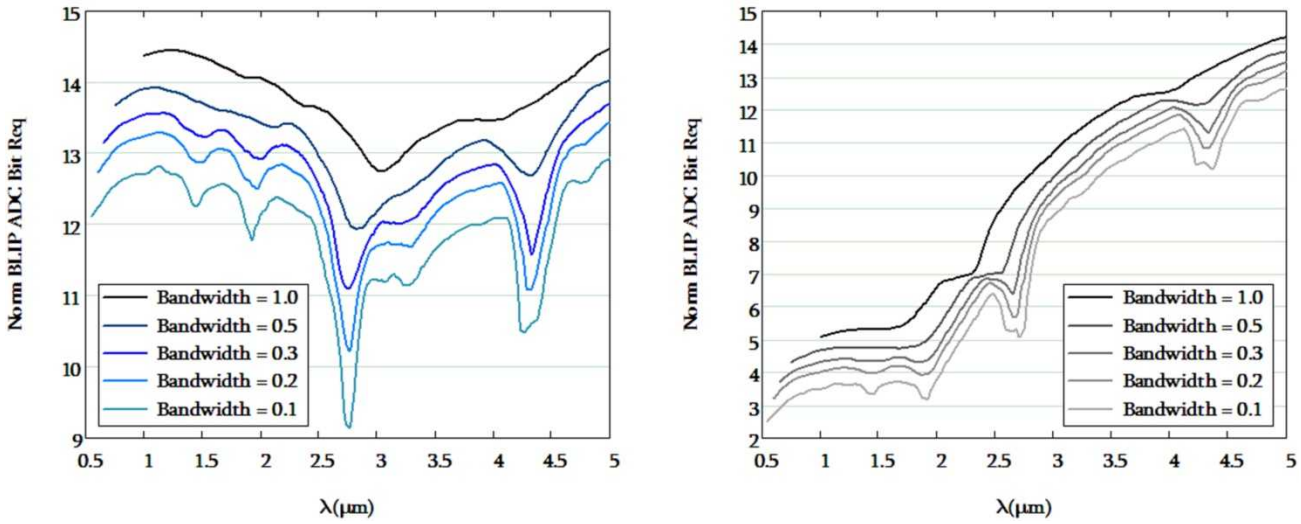

Figure 6. Normalized ADC requirement for maximum Earth backgrounds. Highland noon (left) and full moon midnight (right).

For example, consider a sensor operating at 3.15µm nominal with a 0.3µm bandwidth. The normalized requirement *vs.* maximum background is 12 bits. If no allowance is made for improved performance against lower background levels, $\beta = 1$. Assume peak target is equal to maximum background ($\varepsilon = 1$), the frame rate is 100 Hz, the Airy disc spans two pixels ($n = 2$), and that δ, $\overline{\eta}$, and $\overline{\zeta}_{opt}$ are all 0.8. The correction factor is:

$$N_{corr} = \tfrac{1}{2} \cdot \log_2 \left(\frac{1 \cdot (1+1)^2 \cdot 0.8 \cdot 0.8 \cdot 0.8}{2^2 \cdot 100} \right) \tag{35}$$

Or $N_{corr} = -3.8$, therefore $N_{eff} = 8.2$ or for practical implementation, 9 bits.

A sensor designed to achieve the maximum performance permitted by the instantaneous background, on the other hand, presents a much greater challenge. Figure 7(a) shows the normalized requirement for a sensor operating over the full dynamic range of the background, from daytime highland maximum to nighttime new moon minimum. Except at very high sample frequencies, the bit count requirement will be 20 or more at the shorter wavelengths, and difficult to achieve. The ADC dynamic range challenge can be mitigated by parsing the background into (for example) two (b-c) or three (d-f) parts, provided a dynamically adjustable well capacitance may be integrated into the ROIC circuitry.

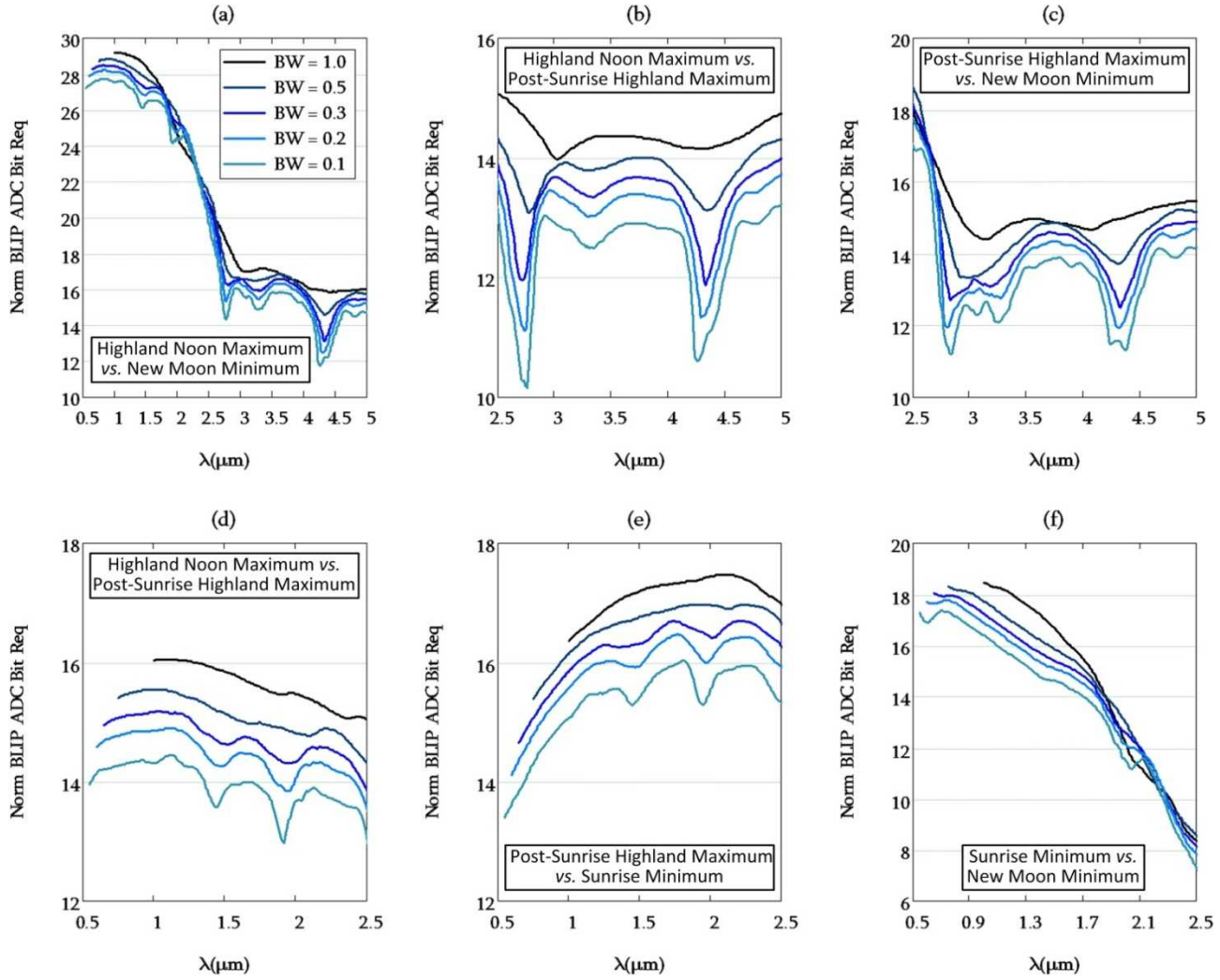

Figure 7. Use of multiple integration well depths to accommodate dynamic range. (a) Full dynamic range, (b-c) high-low dual range for MWIR, (d-f) high-medium-low treble range for Vis-SWIR. Sunrise is defined as a solar zenith angle of 90.833°. Post-sunrise is defined as 1/12 of the duration between sunrise and Noon.

5.3 ADC bit count impacts on system requirements

The pixel counts of FPAs have trended dramatically upward in recent years. Active-pixel designs provide optical detector data in a random-access fashion analogous to computer memory ICs. But these expanded sensing capabilities come at the price of power dissipation adjacent the detector array, an especially important consideration for space based sensors operating in the MWIR, where active cooling is often required. Such cryogenic technologies tend to dissipate an order of magnitude more power than they transport as heat, amplifying the importance of ADC dissipation. Moreover, the empirical power dissipation of high-efficiency ADCs has been shown to be logarithmic with bit count[6], such that 0.1nJ/bit/sample is practicable for a 10-bit ADC, whereas 2nJ/bit/sample is attained for a 16-bit ADC. This nonlinearity underscores the importance of avoiding ADC over-specification in sensor design.

6. CONCLUSIONS

The foregoing examination of space based seeker / warning sensor ROIC ADC requirements is necessarily simplistic. Yet it illustrates the impact of some of the main sensor performance drivers in a generic fashion that is largely independent of specific application objectives, exposing trends across optical band and other key design variables. Use of a consistent design construct matching the detector pixel dimensions to the Airy disc produced by an unresolved target yields nearly constant ADC bit count demands from the visible through the MWIR against maximal Earth background, excepting certain narrow optical bands. Sensors seeking optimal performance throughout the full dynamic range of background radiance face steeper design challenges in the visible to SWIR bands where the day / night differences are more pronounced.

Sandia National Laboratories is a multi-program laboratory operated by Sandia Corporation, a wholly owned subsidiary of Lockheed Martin company, for the U.S. Department of Energy's National Nuclear Security Administration under contract DE-AC04-94AL85000.

REFERENCES

[1] T. S. Lomheim, and E. D. Hernandez-Baquero, "Translation of spectral radiance levels, band choices, and signal-to-noise requirements to focal plane specifications and design constraints." Proc. SPIE 4486, 263-307 (2002).

[2] E. Friedman, and J. L. Miller, [Photonics Rules of Thumb] SPIE Press, 24-26 (2004).

[3] A. M. Baldridge, S. J. Hook, C. I. Grove *et al.*, "The ASTER spectral library version 2.0," Remote Sensing of Environment, 113(4), 711-715 (2009).

[4] A. Berk, G. P. Anderson, P. K. Acharya *et al.*, [MODTRAN4 Version 3 Revision 1 User's Manual], (2003).

[5] R. H. Walden, "Analog-to-Digital Converter Survey and Analysis," IEEE Journal on Selected Areas in Communications, 17(4), 539-550 (1999).

[6] B. Murmann, "A/D converter trends: Power dissipation, scaling and digitally assisted architectures," Custom Integrated Circuits Conference, IEEE, 105-112 (2008).